Low Temperature Physics/Fizika Nizkikh Temperatur, 2020, vol. 46, No. 11, pp. 1336–1345

Nanoindentation of pure and gas-saturated fullerite C_{60} crystals: elastic-to-plastic transition, hardness, elastic modulus

S. N. Dub[1], G. N. Tolmachova[2], S. V. Lubenets[3], L. S. Fomenko[3], and H. V. Rusakova[3]

[1]*V. Bakul Institute for Superhard Materials of the National Academy of Sciences of Ukraine, Kyiv 04074, Ukraine*

[2]*National Science Center "Kharkov Institute of Physics and Technology" of the National Academy of Sciences of Ukraine, Kharkiv 61108, Ukraine*

[3]*B. Verkin Institute for Low Temperature Physics and Engineering of the National Academy of Sciences of Ukraine Kharkiv 61103, Ukraine*

E-mail: lubenets@ilt.kharkov.ua

Received June 18, 2020, published online September 21, 2020

Elastic-plastic transition at nanoindentation of (111) plane of pure C_{60} fullerite single crystals was studied. The onset of plastic deformation in the contact was noted due to the plateau formation in the initial part of loading curve. The estimated stress of plasticity beginning was found to be on the order of the theoretical shear stress required for homogeneous dislocation nucleation in the ideal crystal lattice of C_{60}. The empirical values of elastic modulus $E \approx 13.5$ GPa, hardness of the ideal crystal lattice $H \approx 1.4$ GPa, and hardness at different indentation loads were obtained. The hardness vs load dependence was found consistent with the model of geometrically necessary dislocations. The loading diagrams shape and the dependencies of contact pressure vs indentation depth were strongly affected by gaseous interstitial impurities (hydrogen, oxygen, nitrogen) in C_{60} crystal; transition stress was essentially less and plateaus formation was observed at elevated indentation loads and depths as compared with pure fullerite crystal. For crystals, saturated with hydrogen, the enhanced value of elastic modulus (~ 20.4 GPa) and hardness (~ 1.1 GPa) were obtained. The results acquired at room temperature for C_{60} with face-centered cubic lattice are important for the description of the physical-mechanical properties of simple cubic lattice phase of C_{60} below 260 K (S. V. Lubenets, L. S. Fomenko, V. D. Natsik, and A. V. Rusakova, *Fiz. Nizk. Temp*. **45**, 3 (2019) [*Low Temp. Phys.* **45**, 1 (2019)]).

Keywords: C_{60} fullerite single crystals, nanoindentation, elastic-plastic transition, dislocation nucleation, theoretical shear stress, molecular interstitial impurities.

1. Introduction

Fullerite C_{60} is one of a new class of molecular crystals, structural units of which are the stable fullerenes molecules consisting of 60 carbon atoms. The shape of the C_{60} molecule is a regular truncated icosahedron. The high-temperature crystal phase ($T \geq 260$ K) generated by fullerenes of this type has the symmetry of face-centered cubic (FCC) lattice. The low-temperature phase has a simple cubic (SC) lattice and exists at $T \leq 260$ K. The molecules in these crystal structures are predominantly interconnected by dispersion (van der Waals) forces with a small proportion of covalent bonds. After discovery of fullerenes in 1985 [1] and fullerites synthesis in 1990 [2], a lot of fundamental investigations of structure of fullerenes molecules, mainly C_{60} and C_{70}, as well as structure, phase transitions, different physical properties of C_{60} and C_{70} crystals were realized. It is due to the fact that the fullerites are perspective for application in semiconductor engineering, electronics, medicine and pharmacology.

Basic information on the low temperature physical and mechanical properties of C_{60} and C_{70} fullerites is presented in the review [3]. These fullerites are the softest instances of the molecular crystals. C_{60} crystals grown from the gas phase enhance the capabilities of investigations of mechanical properties: the major part of them was made by indentation and only small amount of experiments was carried out by macrodeformation methods with a constant rate of sample compression. The etching of the (111) habit plane of a single crystal confirmed the dislocation nature of plastic

deformation of C_{60} fullerite (the proposed etchant, toluol [4], does not reveal the growing dislocations). Further researches made it possible to establish the slip system in C_{60} crystals (octahedral system as well as in other FCC structures) and its invariance during FCC → SC phase transition which based on the orientation ordering of fullerene molecules [5, 6], the presence of cleavage along the (111) closest-packed plane [7], the correlation between the temperature dependence of microhardness and the structural phase transformations [3].

Much attention was given to study elastic properties of single crystals and polycrystals of C_{60} in the temperature range from room temperature to 100 K. The results of these investigations and corresponding references are represented in [3]. Ultrasonic methods of measuring of elastic properties showed that Young's modulus of the polycrystalline fullerite at room temperature was about 12 GPa; it is close to Young's modulus of lead but it is significantly less than for other metals. Elastic constant c_{11} of the single crystal is about 15 GPa.

Microindentation of (111) plane and macrodeformation with a constant rate of compression of C_{60} single crystals showed that at room temperature microhardness of the samples varied in the range from 140 MPa to 200 MPa, and yield stress in the <110>{111} slip systems was in the interval from 0.7 MPa to 2.6 MPa. Such differences of the mechanical properties are due to the growth conditions. Irradiation with light, exposure in magnetic field, exposure in air without lighting, special saturation with gas impurities, mechanochemical polishing, pressure treatment of fullerite powder in gaseous medium during compacts preparation and others essentially effect on resistance to plastic deformation of C_{60} fullerite — single crystals and polycrystals [3].

Nanoindentation of epitaxial polycrystalline coating with grain size about 20–30 μm and (111) orientation shown the following results: hardness was (0.55±0.17) GPa, Young's modulus was (15±1) GPa [8]. The high value of hardness is evidently due to the low load on the indenter of 0.2 mN. In this case, it is impossible to exclude the influence of photopolymerization and/or saturation of film surface with atmospheric air molecules. These effects, in particular, can be a reason for the high value of the elastic modulus.

The aim of this work is to study the mechanical properties of single crystals of pure C_{60} fullerite and fullerite saturated with gas impurities by nanoindentation on the (111) habit plane and on the cleavage plane of the same orientation.

2. Experimental procedure

In these investigations reasonable large single crystals of fullerite with (111) habit plane were used. Growing technique of such crystals is described in work [7]. Procedure of saturation of crystals with hydrogen at temperature 250 K and pressure 30 atm is given in works [9, 10]. Measurement of micro- and nanomechanical properties were carried out not only on the (100) and (111) habit planes of the grown crystal but on the (111) plane obtained by cleavage of the crystal. Before nanoindentation, the hydrogen-saturated samples exposed in air at room temperature during about two month, hence they contained not only residual hydrogen but also another gas impurities absorbed from air. For simplicity, we marked these samples as $C_{60}(H_2)_x$ since desorption of hydrogen before measurements was far from complete [9]. Also the fullerite samples after long-term (about 10 years) preservation in evacuated and sealed ampoules were tested; the (111) habit plane and the cleavage planes were indented. The measurements on the cleavage plane were performed in ~ 30 h and in 10 days after sample cleavage.

Microhardness was measured in the load range of 10–100 mN using a standard hardness tester PMT-3 with Vickers pyramid. Tests on nanoindentation of crystals of pure and hydrogen-saturated fullerite were carried out with a three-sided Berkovich indenter on a Nano Indenter-II nanohardness tester (Nano Instrument Inc., Knoxville, TN, USA) at the several specified loads ≤ 10 mN and the load increase rates ≤ 0.2 mN/s in a load control mode. The indenter tip radius is ~ 407 nm according to measurements using atomic force microscope. To determine hardness H and elastic modulus E, the unloading curve of indenter was analyzed according to the generally accepted method of Oliver–Pharr [11]. As a result of such analyze, the contact stiffness S at peak load was found. Knowledge of stiffness makes it possible to define a projection contact area under peak load and consequently hardness and elastic modulus of the sample without measuring of indentation size. The technique proposed in [12–14] was used to obtain the dependence of the average contact pressure p_{mean} (ACP which corresponds to Meyer hardness H_M) vs displacement h.

Nanoindentation of the samples aged in sealed ampoules during about 10 years was performed using Nano Indenter G200 (MTS Systems, Oak Ridge, TN, USA). Tests with this instrument were carried out in the Continuous Stiffness Measurement (CSM) mode [15, 16]. In such mode of nanoindentation, load applied by the loading device is modulated by low frequency and low amplitude signal. As a result, during indenter penetration the portions of short-term load decreasing appears; that makes it possible to obtain the dependences of contact stiffness S and ACP on the displacement at the indenter penetration piece. Load on the Berkovich indenter was increased until indenter displacement reached 225 nm (experiment in the displacement control mode). The tests were performed at the constant strain rate of 0.05 s^{-1}. The CSM signal frequency was 45 Hz, the amplitude oscillation was 2 nm.

Special attention was paid to the initial loading curve piece and the features of elastic-plastic transition in the nanocontact.

3. Experimental results

3.1. Pure fullerite C_{60}: elastic-plastic transition, hardness, elastic modulus

Vickers microhardness H_V in measurements on the (111) habit plane of lamellar single crystals with thickness up to 1 mm and bulk single crystals with sizes 3×4×6 mm in a short time after growing was ~ (0.175±0.03) GPa (for such crystal(s) we will use the term "fresh crystal(s)" too). The same microhardness was obtained when indenting the (111) cleavage plane. Microhardness of (100) plane was as a rule in 1.25–1.5 times less. Scatter of H_V values not only on different samples but in various places of a sample is evidently determined by a defect structure formed during the crystal growth.

More complete information on the mechanical properties of the small-sized samples is provided by experiments on nanoindentation. Typical diagram of Berkovich indenter penetration $P(h)$ (P is a load, h is a penetration depth) for (111) plane of C_{60} fullerite single crystal (shown in the Fig. 1). The diagram was recorded up to the maximum predetermined load of 0.2 mN. The main detail is a plateau (pop-in) in the indenter penetration curve; the plateau corresponds to the stepwise increase in the contact depth. The plateau appeared at the critical load $P_{crit} \approx 0.02$ mN and the depth about 10 nm as a result of sharp increase in indentation depth by 9 nm in a time < 0.17 s (the device measures the load and displacement every 0.17 s). Such pop-ins are well known for high-purity metals single crystals and semiconductors with a specially prepared surface. The surface should be the growth face of the crystal, the fresh cleavage plane or the surface of the sample after electropolishing (i. e., there should be no surface defects). It was established that in plastic materials the pop-in corresponded to an elastic-plastic transition caused by homogeneous nucleation of dislocations in a contact provided that there is no phase transformation initiated by a mechanical load. Until the pop-in is formed, the contact is pure elastic. If the surface of the single crystal is mechanically polished with an abrasive, the pop-in disappears due to the presence of high density of dislocations in the surface layer. In the C_{60} fullerite crystal such pop-in was observed at nanoindentation of a grain of a 20 μm thick film deposited on mica. The grain surface was parallel to the (111) crystallographic plane [8].

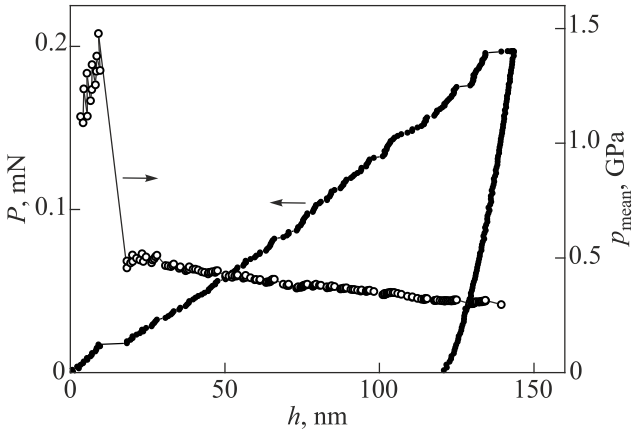

Fig. 1. The typical load-indenter penetration depth P–h diagram and the dependence of the average contact pressure on the indenter penetration depth $p_{mean}(h)$ for the (111) plane of C_{60} single crystal.

Another feature of the penetration curve of the indenter is that at the penetration depths of (100±20) nm periodically repeating numerous smaller pop-ins appear. They are probably caused by the formation of slip lines at the sides of the impression. The pop-ins at the very low indenter loads and accordingly the small indenter penetration depths are essentially the precursors of the unstable deformation observed in many crystalline materials during tension/compression [17]. However it should be noted that the total deformation (elastic + plastic) ε_t in the micro- and nanovolume underneath the impression of pyramidal indenter is several percent (total deformation is determined according to the expression $\varepsilon_t = -\ln(\sin\gamma)$, where γ is the angle between the face and the axis of the pyramid [18]; then for Vickers indenter, regardless of the depth of indenter penetration or on the indenter load $\varepsilon_t \approx 7.6$ %, and for Berkovich indenter $\varepsilon_t \approx 9.8$ %), i. e., corresponds to the developed plastic flow.

After complete unloading of the indenter, the residual imprint with a depth of ~ 120 nm is recorded (Fig. 1), indicating that plastic deformation of the crystal occurred in the contact area at a load of 0.2 mN. The unloading curve shows very weakly defined signs of viscoelasticity, although the viscoelastic behavior is characteristic for materials with significant fraction of van der Waals bonds between molecules and atoms (organic polymers, amorphous selenium [19], single crystals of HOPG (highly oriented pyrolytic graphite) [20], two-dimensional polymers C_{60} obtained at high pressures and temperatures [21]). It can be concluded that C_{60} single crystals are elastic-plastic materials with sufficiently low viscosity.

Information about the change in the resistance to the penetration of the indenter into the material at the loading stage is given by the record of the average contact pressure (ACP) throughout the experiment. The dependence of the ACP on the penetration depth is shown in Fig. 1. In the elastic penetration piece, the ACP increases until the moment of elastic-plastic transition (pop-in formation). Then the ACP sharply decreases from a maximum value of ~ 1.4 GPa to a value of ~ 0.5 GPa and gradually decreases at further load increasing, reaching a value of ~ 0.27 GPa at the indentation depth of ~ 140 nm. The value of 0.27 GPa corresponds to the nanohardness of pure fullerite in this experiment at an indenter load of 0.2 mN.

Tables 1 and 2 show the mechanical characteristics of single crystals of pure and hydrogen-saturated $C_{60}(H_2)_x$ fullerite at maximum predeterminated loads (for a discussion on the latter see Sec. 3.2). Load-penetration depth

diagrams were recorded up to fixed loads of 0.2, 1, and 10 mN which are indicated in the upper rows of the Tables.

Table 1. Mean values of hardness (GPa) at loads of 0.2, 1, and 10 mN

Sample	0.2 mN	1 mN	10 mN
C_{60}	0.27 ± 0.03	0.22 ± 0.00	0.17 ± 0.00
$C_{60}(H_2)_x$	1.31 ± 0.04	1.13 ± 0.08	0.87 ± 0.01

Table 2. Mean values of elastic modulus (GPa) at loads of 0.2, 1, and 10 mN

Sample	0.2 mN	1 mN	10 mN
C_{60}	13.0 ± 0.0	14.1 ± 1.1	13.3 ± 0.1
$C_{60}(H_2)_x$	20.7 ± 1.1	21.8 ± 1.8	18.8 ± 0.1

Let us pay attention to the dependence of the nanohardness value on the indenter load; the nanohardness is higher, the load is less. The elastic modulus does not depend on the load; the average value of the modulus for pure fullerite crystal is ~ 13.5 GPa which is close to the value obtained in ultrasonic measurements, and for fullerite $C_{60}(H_2)_x$, one and a half times higher (~ 20.4 GPa). These issues and the effect of hydrogen and other gas impurities on the mechanical characteristics of the fullerite are considered in the next Section.

3.2. The effect of interstitial gas impurities on the mechanical properties of fullerite

Fullerite readily and reversibly absorbs atoms and molecules of small sizes. The enhanced absorption properties of fullerite are due to weak van der Waals bonds between molecules and the presence of sufficiently large octahedral and tetrahedral voids in the FCC crystal lattice [22]. As a result, interstitial solid solutions are formed with physical and mechanical properties that differ from those of pure fullerite.

It was shown in [9] that the absorption of hydrogen by a single crystal of fullerite led to an increase in the lattice parameter by about 0.2 %; in highly saturated samples, a fourfold increase in microhardness was recorded. Optical microscopy of the $C_{60}(H_2)_x$ showed that in the process of hydrogen saturation, the microstructure of the hydrogen-saturated crystal also changed: an intensive evolution of slipping in the surface layer and the appearance of cracks were revealed; saturation over a long period of time caused destroying the samples [9].

Nanoindentation of $C_{60}(H_2)_x$ crystals was carried out on samples held for a long time under natural conditions in an air atmosphere. In this case, two processes took place: desorption of hydrogen, which caused a drop in microhardness, and counter absorption of gas molecules from the ambient air, which was accompanied by strengthening. Thus, a sample that was saturated with hydrogen at a temperature of 250 °C and a pressure of 30 atm for 900 h had a microhardness of ~ 0.57 GPa, and after holding at room temperature in an air atmosphere for 170 h its hardness decreased to ~ 0.4 GPa; then subsequent exposure for about 2 months led to an increase in hardness up to ~ 0.54 GPa. The kinetics of these processes has been studied in detail and described in [3, 9, 10]. The data in Tables 1 and 2 refer to the test of a similar specimen that has passed all of the above procedures. They show the total effect of interstitial gas impurities on the mechanical properties of fullerite and indicate not only a significant increase in hardness (by a factor of 5 when the indenter load is 10 mN), but, as expected [9], a significant change in the elastic modulus. As seen in the Table 2, the modulus of elasticity changed from 13.3 GPa in pure fullerite to 18.8 GPa in a $C_{60}(H_2)_x$ crystal, i. e., increased by 1.4 times.

Figure 2 shows the $P(h)$ diagrams within the peak loads of 0.2 and 10 mN during the indentation of the $C_{60}(H_2)_x$ sample and, for comparison, a sample of pure C_{60} fullerite. After unloading of the indenter, a residual imprint with a depth of > 30 nm was observed in the $C_{60}(H_2)_x$ crystal at a maximum load of 0.2 mN [Figs. 2(a) and 2(b)] and ~ 600 nm at a maximum load of 10 mN [Fig. 2(c)], as evidence of the plastic deformation that took place in the contact. The curves of the indenter penetration do not contain pop-ins, which are clearly fixed during the indentation of pure fullerite, in which they are associated with homogeneous nucleation of dislocations in a perfect lattice. The whole dependence $P(h)$ in the case of intercalated fullerite [Fig. 2(a)], has the form of a curve describing the elastic-plastic deformation of the crystal at the contact area during the entire loading period, starting from the moment when the indenter touched the sample. In the $P(h)$ diagram, one can see fuzzy displacement discontinuities [Fig. 2(b)], which correlate with stress drops < 0.1 GPa in the $p_{mean}(h)$ diagram [Fig. 2(b)]. An abrupt instability of plastic deformation is also observed during indentation up to a load of 10 mN [Fig. 2(c)]. This character of elastic-plastic deformation was also observed at indentation of pure fullerite, but only after pop-ins corresponding to the transition from a purely elastic contact of the indenter with a crystal to an elastic-plastic flow of the material under the indenter. In Figs. 2(a) and 2(b) the corresponding drops and pop-ins are marked with arrows.

The strengthening of fullerite as a result of absorption of hydrogen, as noted above, led to the embrittlement of the crystal. During nanoindentation of the $C_{60}(H_2)_x$ sample, even under conditions of moderate concentrated mechanical impacts, radial cracks appeared along the (111) cleavage planes, which propagated from the indentation to sample edges.

The character of deformation during nanoindentation of fullerite is influenced not only by the temperature and pressure enhanced absorption of gas impurities (in our case, hydrogen), but also by other factors. The $P(h)$ diagram of a sample of pure fullerite C_{60}, which was stored in an evacuated sealed ampoule for 10 years, significantly differs from the nanoindentation diagram of a sample that

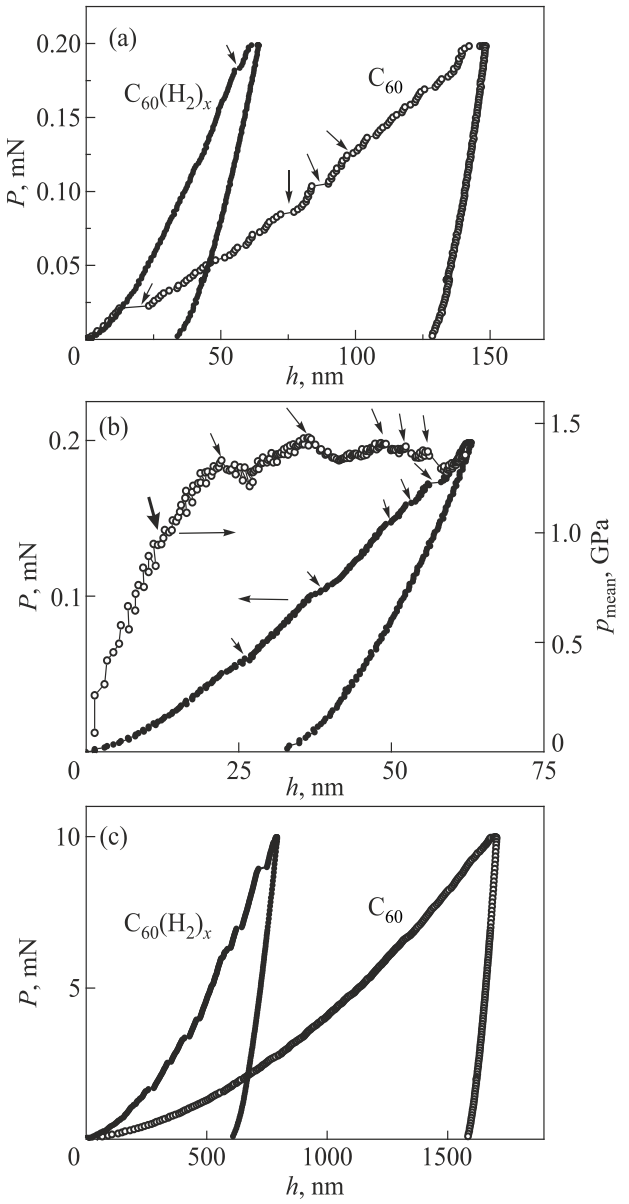

Fig. 2. (a) The load-indenter penetration depth *P*–*h* diagrams for the (111) plane of C_{60} and $C_{60}(H_2)_x$ single crystals. The predetermined load is 0.20 mN. The arrows point to the pop-ins in the *P*(*h*) curves. (b) The load-indenter penetration depth *P*–*h* diagram and the dependence of the average contact pressure on the indenter penetration depth $p_{mean}(h)$ for the (111) plane of $C_{60}(H_2)_x$ single crystal. The predetermined load is 0.20 mN. Thick arrow points to the end of the elastic piece. (c) The load-indenter penetration depth diagrams for the (111) plane of C_{60} and $C_{60}(H_2)_x$ single crystals. The predetermined load is 10 mN.

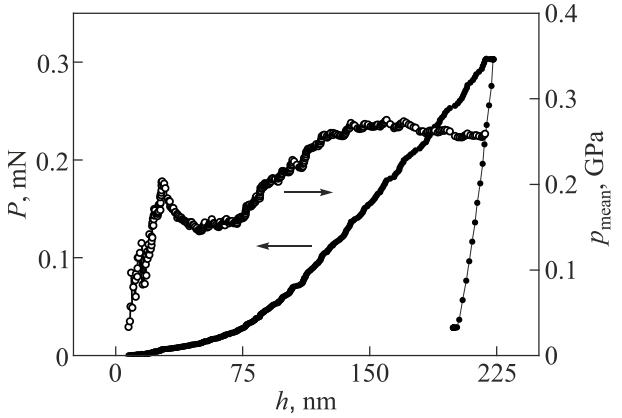

Fig. 3. The load-indenter penetration depth *P*–*h* diagram and the dependence of the average contact pressure on the indenter penetration depth $p_{mean}(h)$ for the (111) plane of C_{60} single crystal that was in vacuum sealed ampoule during 10 years.

was stored in the ampoule for a much shorter time (about 2 months — Fig. 1). One of the typical *P*(*h*) diagrams for an aged (10-year-old) crystal is shown in Fig. 3. The dependence of the ACP on the penetration depth (Fig. 3) clearly shows the initial elastic deformation piece to a depth of ~ 30 nm at a small value of the ACP of ~ 0.2 GPa. Note that for a fresh sample of pure fullerite at the end of the elastic piece before pop-in formation ACP was equal to ~ 1.4 GPa (Fig. 1). After a sharp decrease, the ACP gradually increased to a value of ~ 0.27 GPa (Fig. 3). This is the hardness of aged fullerite, which was determined by indentation to a maximum specified load of 0.3 mN. The elastic-to-plastic transition in the nanocontact is smooth and pop-in is not recorded in the indenter penetration diagram *P*(*h*). The average value of the elastic modulus of this sample is $\bar{E} \approx 13.61$ GPa. As can be seen, the elastic modulus and hardness of the crystal retained their values during long-term storage in the ampoule, but the indentation diagrams *P*(*h*) and $p_{mean}(h)$ changed significantly.

This behavior (the absence of pop-in indicating an elastic-plastic transition) was observed, as noted above, during the indentation of a hydrogen-saturated $C_{60}(H_2)_x$ sample. During the long-term storage of fullerite in the ampoule, a change in the properties of the crystal, at least of its surface layer, occurred apparently due to the absorption of residual gas molecules.

The environment is a source of gaseous impurities, mainly nitrogen and oxygen molecules, which fullerite can absorb and change its physical and mechanical properties [22]. The absorption process is quite fast even at room temperature; after holding for several hours, especially under illumination, the hardness of the crystal can increase significantly [3].

The diagrams of nanoindentation of the cleavage plane of a sample stored for 10 years in an ampoule, and then after cleavage for about 30 h in natural conditions in the dark, are shown in Fig. 4. As can be seen, there are no signs of transition from elastic deformation to elastic-plastic flow in the form of a pop-in in the diagram *P*(*h*) (in this respect, Figs. 3 and 4 are similar). In this case, the $p_{mean}(h)$ diagram nevertheless shows an elastic piece up to an indentation depth of ~ 35 nm, after which a penetration region of ~ 20 nm was observed at a constant average contact

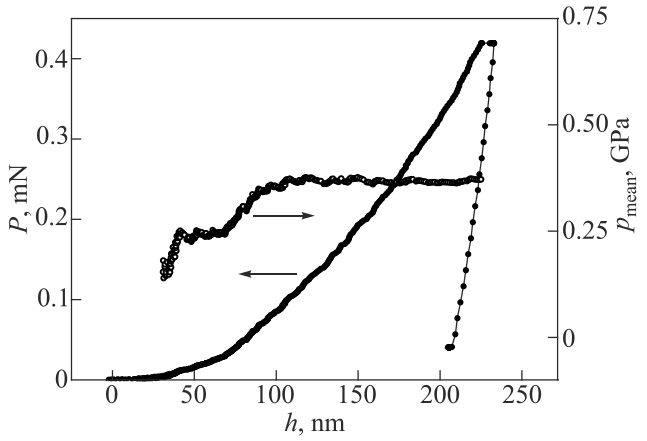

Fig. 4. The load-indenter penetration depth P–h diagram and the dependence of the average contact pressure on the indenter penetration depth $p_{mean}(h)$ for the cleavage (111) plane of C_{60} single crystal, that was in vacuum sealed ampoule during 10 years and after cleavage was in darkness under natural conditions during about 30 h.

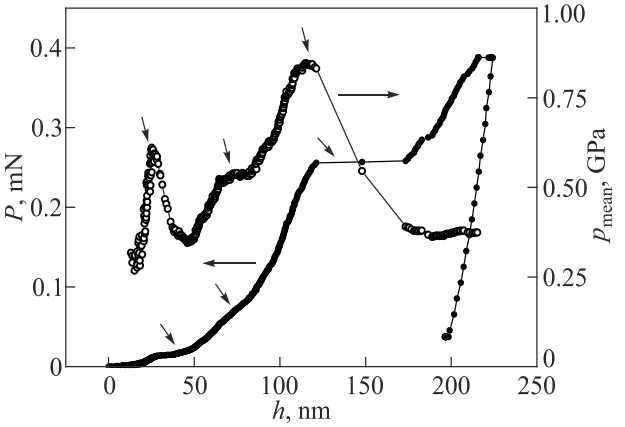

Fig. 5. The load-indenter penetration depth P–h diagram and the dependence of the average contact pressure on the indenter penetration depth $p_{mean}(h)$ for the (111) cleavage plane of C_{60} single crystal, that after cleavage was in darkness under natural conditions during 10 days. The arrows point to the diagram piece where the pop-ins are fixed.

pressure of ~ 0.25 GPa, followed by a transition to elastic-plastic deformation with hardening. In Fig. 3, the elastic piece was followed by a sharp decrease in p_{mean}. At the maximum load of ~ 0.43 mN, the average values of the elastic modulus $\bar{E}$ = 15.6 GPa and hardness $\bar{H}$ = 0.4 GPa were obtained, which show that when a fresh cleavage is kept in air, there was a noticeable hardening of the surface layer of the crystal, as well as a change in the character of the indentation diagrams.

The mechanical behavior of a sample at indentation of the cleavage plane after exposure to air for several days (the samples were tested after 7 and 10 days of exposure) is qualitatively different from that described in the previous paragraph. One of the main differences is the appearance of pop-ins in the $P(h)$ diagram. However, the pop-ins were fixed at large depths 100–150 nm at critical loads from 0.12 mN to 0.25 mN; penetration depth jumps in the contact reached 50 nm. The nature of these jumps and jumps observed during the indentation of a fresh crystal is obviously different. The main features of the indentation diagrams of the sample after 10 days of exposure are illustrated in Fig. 5. In the $P(h)$ diagram, one can see a weakly pronounced pop-in, indicated by an arrow, similar to that clearly observed in Fig. 1 for a fresh sample, with the same load on the indenter ~ 0.02 mN, but at a larger indenter penetration depth of ~ 25 nm. The $p_{mean}(h)$ diagram shows an elastic contact piece to a depth of ~ 25 nm. In this case, the ACP reached a maximum value of ~ 0.6 GPa, which is 2.3 times less than in a similar situation in a fresh fullerite crystal (1.4 GPa). Then, the ACP decreased to ~ 0.35 GPa, after which it began to rise with the exit to the inhomogeneous elastic-plastic deformation of the material under the indenter. The plateau in the $p_{mean}(h)$ diagram corresponds to the nonmonotonic deformation piece in the $P(h)$ curve, marked with an arrow. A large penetration depth jump in the contact at a depth of ~ 120 nm is associated with a decrease in the ACP from ~ 0.85 GPa to ~ 0.4 GPa. In this case, the modulus of elasticity changed from ~ 20 GPa to ~ 15 GPa. The latter values correspond to the hardness and elastic modulus, measured on the cleavage plane of the crystal after 10 days of exposure in natural conditions (in air, and in the dark). The maximum specified load on the indenter was ~ 0.4 mN.

The indentation of the cleavage plane after 7-day exposure revealed the following features in the indentation diagrams: the elastic deformation piece was observed to a depth of ~ 50 nm, after which the deformation under the indenter had an inhomogeneous elastic-plastic character with an increase in the ACP value. The loading diagram $P(h)$ did not reveal any signs of a penetration depth jump at a low load, which could be compared with the $p_{mean}(h)$ dependence and taken as an elastic-to-plastic transition. The elastic modulus and hardness, on average, had the following values, indicating the hardening of the surface layer: $\bar{E}$ = 15.9 GPa and $\bar{H}_M$ = 0.48 GPa. These values differ little from those measured on the cleavage plane after a 30-hour exposure of the cleavage in air.

Experiments on microindentation of all the samples listed above showed that the hardening revealed at nanoindentation of the cleavage plane of samples exposed to air refers only to changes in the mechanical properties of the surface layer. The average value of microhardness at a load on the indenter of 100 mN, which corresponds to the depth of penetration of the indenter $h \approx 17$ μm, was within 0.13–0.15 GPa, did not depend on the exposure time in air or on the mechanochemical polishing of the sample surface, and did not differ from the measured value on the habit plane of a fresh crystal. Only at low loads ≤ 0.02 N the microhardness of samples exposed to air or mechanochemical polished was higher than that of a fresh crystal.

4. Discussion

4.1. On the nucleation of slip in a pure fullerite crystal during nanoindentation

In Sec. 2, it was noted that the Berkovich indenter tip was becoming blunt as a result of prolonged operation, its shape became close to spherical with a radius of $R \approx 407$ nm. The initial elastic section of the loading curve can be analyzed therefore using the analytical Hertz solution to the problem of the contact between a rigid sphere and a flat surface. For this case, Hertz's theory gives the following expression for the dependence of the average contact pressure p_{mean} on the indenter load P, the indenter radius of sphere R, and the elastic properties of the contacting materials [23, 24]:

$$p_{\text{mean}} = \left(\frac{16PE_r^2}{9\pi^3 R^2} \right)^{1/3}. \qquad (1)$$

The quantity E_r combines the modulus of the indenter and the specimen:

$$\frac{1}{E_r} = \frac{1-\nu_i^2}{E_i} + \frac{1-\nu_s^2}{E_s},$$

E_r is the reduced modulus of the system, ν is the Poisson's ratio, the indexes i and s point to the quantities applied to the indenter and specimen. The shear stresses reach the maximum value $\tau_{\max}$ under the contact center at a distance $0.48a$ from the specimen surface (a is the radius of the contact region). They are connected with the maximum pressure $p_{\max}$ by the relation [23]:

$$\tau_{\max} = [0.61 - 0.23(1 + \nu)]\, p_{\max}, \qquad (2)$$

where the Poisson's ratio for fullerite $\nu = 0.306$ [3, 25]. In turn, the maximum pressure is one and a half times the average contact pressure $p_{\max} = \frac{3}{2} p_{\text{mean}}$. Then for fullerite we have $\tau_{\max} \approx 0.464\, p_{\text{mean}}$.

For a pure fullerite crystal (Fig. 1 — the (111) indentation plane) at an indenter load of about 0.02 mN a plateau corresponding to an elastic-plastic transition is recorded on the $P(h)$ curve. At the onset of the transition the average contact pressure reached its maximum value $p_{\max} = 1.4$ GPa (Fig. 1), which, according to Eq. (2), corresponds to the maximum shear stress $\tau_{\max} \approx 0.65$ GPa. Young's modulus determined in the nanoindentation experiment is 13.5 GPa and the shear modulus is $G = 5.17$ GPa at $\nu = 0.306$. Knowing the value of the shear modulus, we obtain an estimate of the theoretical shear strength according to Frenkel [26] $\tau_{\text{teor}} = G/(2\pi) = 0.82$ GPa. For a number of reasons, this value is considered as overestimated, and the more acceptable value of the stress required for the onset of plastic flow is $\frac{1}{15}G$ [27] or for fullerite $\tau_{\text{teor}} = 0.34$ GPa. It can be seen that the maximum shear stress in the contact at the onset of the plastic flow is close to the average estimated value of the theoretical shear strength of the crystal. It can be argued that the elastic-plastic transition (the formation of a pop-in on the penetration curve of the indenter $P(h)$) is caused by the homogeneous nucleation of dislocations in the contact in the perfect region of crystal, and not by triggering of dislocation sources such as Frank–Read sources. The average contact pressure $p_{\text{mean}} = 1.4$ GPa at the moment of pop-in formation corresponds to the maximum hardness of the (111) plane for a given single crystal. This is the hardness of the ideal crystal lattice of fullerite in the [111] direction.

It is seen in Table 1 that the nanohardness of fresh fullerite depends on the indenter load. This can be considered as a manifestation of the well-known indentation size effect (ISE) [27]. To describe the dependence of the hardness of crystalline materials on the depth of indenter penetration, a simple model proposed earlier [28, 29] was used and developed in [30], which made it possible to describe the formation of an imprint using geometrically necessary dislocations. Within the framework of this model, it is assumed that the resistance to plastic deformation is determined by the total density of statistically accumulated dislocations (SADs) and geometrically necessary dislocations (GNDs) $\rho_t = \rho_s + \rho_G$. In this case, the relationship between the hardness and the penetration depth of the indenter is described by the following expression [30]:

$$\frac{H_M}{H_{M0}} = \sqrt{1 + \frac{h^*}{h}}, \qquad (3)$$

where H_{M0} is the hardness in the absence of GNDs, $\rho_G = 0$, i. e., at $h \gg h^*$, when the deformation gradient under the indenter does not affect the value of the hardness, h^* is the characteristic length which depends on the shape of the indenter, shear modulus, and SADs density ρ_s and characterizes the dependence of hardness on a depth of the indenter penetration.

Figure 6 shows the dependence of the hardness of a pure fullerite crystal on the penetration depth of the indenter in the coordinates $H_M^2 - 1/h$. The data have been obtained by measuring microhardness on the fresh cleavage plane and nanohardness on the habit plane of a fresh sample (two points marked with arrows). Good agreement between the experimental data and Eq. (3) is seen. The parameters of the dependence are as follows: $H_{M0} = 0.143$ GPa, $h^* = 0.61$ μm. The value of H_{M0} is within the measured values of hardness H_V at the maximum load on the indenter, and the parameter h^*, according to the model [30], corresponds to the average density of statistically accumulated dislocations $\rho_s = 3 \cdot 10^{10}$ cm^{-2}.

Thus, experiments on nanoindentation made it possible to obtain the following important mechanical characteristics of pure C_{60} fullerite: the average value of the elastic modulus is 13.5 GPa, the average value of the hardness is 0.17 GPa at a load of 10 mN, the hardness of the ideal crystal lattice is 1.4 GPa, and the shear strength is 0.65 GPa — the stress required for homogeneous initiation of slip in a defect-free lattice, which is comparable to the theoretical strength of an ideal lattice. The dependence of the hardness

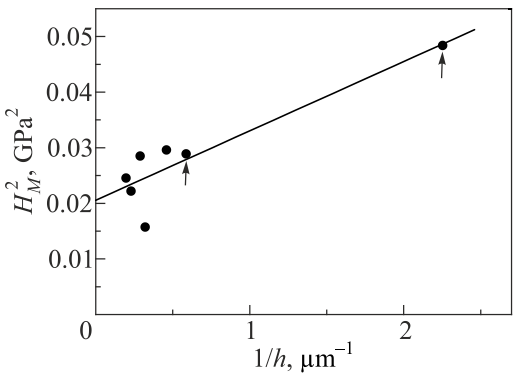

Fig. 6. The dependence of hardness on the indenter penetration depth according to the Eq. (3). The (111) indentation plane is obtained by cleavage of pure fullerite single crystal. Nanoindentation data at loads of 1 and 10 mN are indicated with arrows.

of a pure fullerite single crystal on the indenter load can be described within the framework of the model of geometrically necessary dislocations [30]. The average values of nanohardness (the depth of indenter penetration 1.4 μm) and microhardness (the depth of indenter penetration 17 μm) as the mechanical characteristics of the surface layer and the volume of the crystal are close in magnitude.

4.2. Hardening of fullerite with gas impurities

An increase in the hardness and elastic modulus of fullerite as a result of the absorption of gaseous impurities can be caused by a number of factors, namely, a change in the forces of intermolecular interaction, the formation of a wide range of potential barriers to the motion of dislocations, an increase in the density of dislocations due to relaxation of stresses in regions with high values of the concentration gradient of absorbed molecules, blocking of dislocations as a result of the formation of Cottrell atmospheres. Chemical interaction of impurities with C_{60} molecules is also possible, including the formation of polymer bonds.

The change in the mechanical properties of fullerite crystals was especially pronounced at the hydrogen saturation under conditions of elevated temperature and pressure. Such crystals had high values of micro- and nanohardness and elastic modulus. The long-time saturation of crystals in such conditions led to their destruction without the application of external efforts. This is evidently associated with the formation of a significant gradient of hydrogen concentration and, accordingly, with an increase in the lattice parameter in the surface layer which resulted in the formation of internal tensile stresses, the initiation and development of cracks. Nanoindentation of samples that retained their integrity upon hydrogen saturation led to the formation of cracks along cleavage planes near the indentation even at low loads.

High values of the microhardness of the $C_{60}(H_2)_x$ solid solution persisted in the low temperature range of 77–300 K [9]. Hydrogen saturation led to a significant change in the temperature dependences of the microhardness and the crystal lattice parameter, especially in the region of the FCC → SC phase transition. The transition temperature decreased by about 30 K, and the transition became strongly extended in temperature. The data on the value of the hardness and the dependence $H_V(T)$ indicate a significant change in the intermolecular binding forces and the nature of the dislocation-orientation interaction in the $C_{60}(H_2)_x$ crystal in comparison with the pure C_{60} fullerite crystal.

The hardening of fullerite crystals is an important but not the only effect that was observed during intercalation of gas impurities. As shown in Sec. 3, the nanoindentation diagrams of a crystal saturated with hydrogen or environmental molecules (mainly O_2 and N_2) and a pure fullerite crystal differ significantly. The indenter penetration curves $P(h)$ do not show signs of slip initiation at low loads in the form of pop-in, as that is in case of indentation of a pure fullerite crystal (Fig. 1).

Let us consider the diagrams $P(h)$ and $p_{mean}(h)$ recorded during nanoindentation of the $C_{60}(H_2)_x$ crystal. As seen in [Fig. 2(a)] the diagrams of the initial deformation piece of pure and hydrogen-saturated fullerite crystals coincide up to a load of ~ 0.02 mN and to an indenter displacement of ~ 15 nm. In a pure fullerite crystal after these values of P_{crit} and h a pop-in appeared on the $P(h)$ diagram and the deformation under the indenter assumed an elastic-plastic character. The first noticeable abrupt increase in the penetration depth and a decrease in the ACP [Fig. 2(b)] during nanoindentation of the $C_{60}(H_2)_x$ crystal was observed at higher values of the load and the penetration depth. In this case, the average contact pressure reached the maximum value $p_{max} \approx 1.35$ GPa [Fig. 2(b)], which according to Eq. (2) corresponds to the maximum shear stress $\tau_{max} \approx 0.63$ GPa provided that the Poisson's ratio has the same value $\nu = 0.306$. However, the initial elastic piece as can be seen in the Fig. 2(b) ended before the onset of developed plastic deformation in the contact, and the corresponding value of the ACP is equal to ~ 1 GPa $\approx 0.8\, p_{max}$ (see the thick arrow) . Then we have the value of the maximum shear stress $\tau_{max} \approx 0.46$ GPa. Based on the average value of the elastic modulus $\bar{E} \approx 20.4$ GPa (Table 2), we obtain the value of the shear modulus $G \approx 7.81$ GPa and, accordingly, the theoretical shear stress $\tau_{teor} = G/2\pi = 1.24$ GPa [26] or $\tau_{teor} = \frac{1}{15} G = 0.52$ GPa [27]. Although the value of τ_{max} at transition to an elastic-plastic flow differs little from the estimate of τ_{teor} [27], it can hardly be unambiguously asserted that it corresponds to the stress of nucleation of dislocations in the ideal lattice of a $C_{60}(H_2)_x$ crystal which has many structural defects of impurity (hydrogen and its complexes) and dislocation nature.

The distinctive features of the indenter penetration diagrams for crystals that have absorbed gas impurities from

the environment are described in detail in Sec. 3. The transition between the initial elastic piece of deformation and subsequent plastic flow was carried out smoothly, without pop-in appearing in the loading curve. The onset of the plastic flow of the material under the indenter could be revealed only from the sharp change in the $p_{mean}(h)$ dependence; in this case, p_{mean} reached a value of 0.2–0.6 GPa which is significantly less than in a pure fullerite crystal. Such p_{mean} values do not correspond to the onset of slip in an ideal lattice. An increase in the zone of constrained plastic deformation of the crystal surrounded by an elastically deformed material with a further increase in the load on the indenter occurred with hardening. The average values of hardness and elastic modulus both in the $C_{60}(H_2)_x$ crystal and in the samples intercalated with the molecules of the environment were higher than in the pure fullerite crystal.

The absence of pop-in in the loading curves was noted by the authors of [31] at nanoindentation of a n-ng cBN polycrystal (near-nanograined cubic boron nitride the structure of which is close to nanocrystalline). Additional experiments showed that, in this case, in the initial loading piece in the contact zone elastic penetration of the indenter occurred, and then a gradual transition from elastic deformation to the stage of developed plasticity occurred.

A detailed study of the features of the elastic-plastic transition during nanoindentation of a pure iron polycrystal [32] made it possible to establish that the pop-in phenomenon is influenced by the density of dislocations, grain boundaries, interstitial atoms, and surface defects.

The data on nanoindentation of a fullerite crystal have shown that even a small number of interstitial molecules absorbed from the environment can lead not only to the hardening of the surface layer and the absence of pop-in at low loads, but also to the appearance of significant plateaus of ~ 50 nm in the loading diagrams at a higher load and a greater depth of penetration of the indenter (Fig. 5) than in a pure crystal (Fig. 1).

5. Conclusion

In this work, the mechanical properties of single crystals of fullerite C_{60} have been studied by the nanoindentation. The following results were obtained. For a pure crystal, the average value of the elastic modulus is 13.5 GPa, the average value of the hardness is 0.17 GPa, the hardness of the ideal crystal lattice is 1.4 GPa, and the shear stress is 0.65 GPa — the stress comparable to the theoretical strength of the ideal lattice ($G/(2\pi) > \tau_{max} > \frac{1}{15}G$), i. e., necessary for the homogeneous nucleation of slip in a defect-free crystal. The dependence of the hardness on the indenter load can be described within the framework of the model of geometrically necessary dislocations. The average values of nanohardness at an indenter penetration depth of 1.4 μm and microhardness at an indenter penetration depth of 17 μm, as the mechanical characteristics of the surface layer and the crystal volume, are similar in magnitude. The absorption of the gas impurities led to the hardening of the crystal which resulted in increase of elastic modulus and hardness.

In the case of a high hydrogen concentration, the crystal exhibited brittle behavior: even at low loads, cracks appeared along the cleavage planes. The noted absence of pop-in in the $P(h)$ curves at low loads is associated with a high density of dislocations (notably in a $C_{60}(H_2)_x$ crystal) and with presence of interstitial impurities. The transition from the initial elastic deformation to the subsequent plastic flow occurred smoothly, without an abrupt increase in the penetration depth of the indenter. During nanoindentation of crystals that had contact with the air atmosphere, significant plateaus were observed at increased loads and large indentation depths. These facts indicate a high sensitivity of the mechanical behavior of C_{60} fullerite single crystals to presence of structural defects — dislocations and interstitial gas impurities. Long-term storage of the grown crystals in evacuated and sealed ampoules led to a change in their physical-mechanical properties.

The authors of S. V. Lubenets, L. S. Fomenko, and H. V. Rusakova are grateful to Prof. V. D. Natsik for helpful comments on the text of the manuscript. This work was carried out with a partial support of the KPKVK 6541230 program “The support of the development of priority lines of scientific investigations”.

1. H. W. Kroto, J. R. Heath, S. C. O’Brien, R. F. Curl, and R. E. Smalley, *Nature* **318**, 162 (1985).
2. W. Krätschmer, L. D. Lamb, K. Fostiropoulos, and D. R. Huffman, *Nature* (*London*) **347**, 354 (1990).
3. S. V. Lubenets, L. S. Fomenko, V. D. Natsik, and A. V. Rusakova, *Fiz. Nizk. Temp.* **45**, 3 (2019) [*Low Temp. Phys.* **45**, 1 (2019)].
4. V. I. Orlov, V. I. Nikitenko, R. K. Nikolaev, I. N. Kremenskaja, and Yu. A. Osipyan, *JETF Lett.* **59**, 704 (1994).
5. L. S. Fomenko, V. D. Natsik, S. V. Lubenets, V. G. Lirtsman, N. A. Aksenova, A. P. Isakina, A. I. Prokhvatilov, M. A. Strzhemechny, and R. S. Ruoff, *Fiz. Nizk. Temp.* **21**, 465 (1995) [*Low Temp. Phys*. **21**, 364 (1995)].
6. M. Tachibana, H. Sakuma, M. Michiyama, and K. Kojima, *Appl. Phys. Lett.* **67**, 2618 (1995).
7. S. V. Lubenets, L. S. Fomenko, A. I. Izotov, R. K. Nikolaev, Yu. A. Osipyan, and N. S. Sidorov, *Phys. Solid State* **47**, 891 (2005).
8. V. E. Pukha, A. N. Drozdov, A. T. Pugachov, and S. N. Dub, *Funct. Mater.* **14**, 209 (2007).
9. L. S. Fomenko, S. V. Lubenets, V. D. Natsik, Yu. E. Stetsenko, K. A. Yagotintsev, M. A. Strzhemechny, A. I. Prokhvatilov, Yu. A. Osipyan, A. I. Izotov, and N. S. Sidorov, *Fiz. Nizk. Temp.* **34**, 86 (2008) [*Low Temp. Phys.* **34**, 69 (2008)].
10. K. A. Yagotintsev, I. V. Legchenkova, Yu. E. Stetsenko, P. V. Zinoviev, V. N. Zoriansky, A. I. Prokhvatilov, and M. A. Strzhemechny, *Fiz. Nizk. Temp*. **38**, 1202 (2012) [*Low Temp. Phys.* **38**, 952 (2012)].
11. W. C. Oliver and G. M. Pharr, *J. Mater. Res.* **7**, 1564 (1992).

12. N. V. Novikov, S. N. Dub, Yu. V. Milman, I. V. Gridneva, and S. N. Chugunova, *Sverkhtverdye Materialy* **18**, 36 (1996).
13. S. N. Dub, Y. V. Milman, D. V. Lozko, and A. N. Belous, *MRS Symposium Proc*., *Fundamentals of Nanoindentation and Nanotribology II*, S.P. Baker, R. F. Cook, S. G. Corcoran, and N. R. Moody (eds.), Pittsburgh (2001), Vol. 649, p. Q7.12.1.
14. S. Dub, N. Novikov, and Y. Milman, *Philos. Mag. A* **82**, 2161 (2002).
15. B. Bhushan and X. Li, *Int. Mater. Rev.* **48**, 125 (2003).
16. J. Hay, P. Agee, and E. Herbert, *Exp. Tech.* **3**, 86 (2010).
17. V. V. Pustovalov and V. S. Fomenko, *Plasticheskaya deformatsiya krystallov pri nizkikh temperaturakh*, Naukova Dumka, Kiev (2012).
18. Yu. V. Milman, B. A. Galanov, and S. I. Chugunova, *Acta Metall. Mater.* **41**, 2523 (1993).
19. M. L. Trunov, V. S. Bilanich, and S. N. Dub, *Tech. Phys.* **52**, 1298 (2007).
20. S. N. Dub and E. Kats, *Unpublished results*.
21. A. Dzwilewski, A. Talyzin, G. Bromiley, S. Dub, and L. Dubrovinsky, *Diam. Relat. Mater*. **16**, 1550 (2007).
22. B. Sundqvist, *Fiz. Nizk. Temp.* **29**, 590 (2003) [*Low Temp. Phys.* **29**, 440 (2003)].
23. K. L. Jonhson, *Contact Mechanics*, Cambridge University Press, Cambridge (1985).
24. V. K. Grigorovich, *Tverdost' i microtvrerdost' metallov*, Nauka, Moscow (1976).
25. N. P. Kobelev, R. K. Nikolaev, Ya. M. Soifer, and S. S. Khasanov, *Phys. Solid State* **40**, 154 (1998).
26. J. Frenkel, *Z. Phys.* **37**, 572 (1926).
27. J. P. Hirth and J. Lothe, *Theory of Dislocations*, McGrow HillBook Company, Oslo University (1968).
28. N. A. Stelmashenko, M. G. Walls, L. M. Brown, and Yu. V. Milman, *Acta Metall. Mater.* **41**, 2855 (1993).
29. M. S. De Guzman, G. Neubauer, P. Flinn, and W. D. Nix, *Mater. Res. Soc. Symp. Proc.* **308**, 613 (1993).
30. W. Nix and H. Gao, *J. Mech. Phys. Solids* **46**, 411 (1998).
31. S. N. Dub, I. A. Petrusha, V. M. Bushlya, T. Taniguchi, V. A. Belous, G. N. Tolmacheva, and A. V. Andreev, *J. Superhard Mater.* **39**, 88 (2017).
32. F. Pöhl, *Sci. Rep.* **9**, 15350 (2019).

Наноіндентування чистих та насичених газовими домішками кристалів фулериту C_{60}: пружно-пластичний перехід, твердість, модуль пружності

С. М. Дуб, Г. М. Толмачова, С. В. Лубенець, Л. С. Фоменко, Г. В. Русакова

Вивчено пружно-пластичний перехід у разі наноіндентування площини (111) кристала чистого фулериту C_{60}. Початок пластичної деформації матеріалу під індентором фіксували за появою плато на початковій стадії кривої навантаження. Встановлено, що напруження початку пластичності відповідає величині теоретичного напруження зсуву, необхідного для гомогенного зародження дислокацій в ідеальній кристалічній гратці C_{60}. Одержано емпіричні значення модуля пружності $E \approx 13{,}5$ ГПа, твердості ідеальної кристалічної ґратки $H \approx 1{,}4$ ГПа та твердості при різних навантаженнях на індентор. Залежність твердості від навантаження відповідає моделі геометрично необхідних дислокацій. На форму діаграм навантаження і залежність контактного тиску від глибини індентування сильно впливає наявність у кристалі газових домішок проникнення (водню, кисню, азоту); напруження переходу до пластичності значно менше, формування сходинок спостерігалось при підвищених напруженнях і більших глибинах проникнення індентора у порівнянні з чистим кристалом C_{60}. Для кристалів, насичених воднем, одержано підвищені величини модуля пружності $\sim 20{,}4$ ГПа та твердості $\sim 1{,}1$ ГПа. Дослідження проведено при кімнатній температурі на кристалах C_{60} з гранецентрованою кристалічною ґраткою (високотемпературна фаза), але його результати мають важливе значення для опису фізико-механічних властивостей низькотемпературної фази C_{60} (проста кубічна ґратка) нижче 260 К (С. В. Лубенец, Л. С. Фоменко, В. Д. Нацик, А. В. Русакова, *ФНТ* **45**, 3 (2019) [*Low Temp. Phys.* **45**, 1 (2019)]).

Ключові слова: монокристали фулериту C_{60}, наноіндентування, пружно-пластичний перехід, зародження дислокацій, теоретичне напруження на зсув, молекулярні домішки проникнення.